NJC

New Journal of Chemistry

A journal for new directions in chemistry

Accepted Manuscript

This article can be cited before page numbers have been issued, to do this please use: E. Zhan, F. Wang, J. Wang, Y. Sun, J. Yang, C. Zhang, J. Kong, L. Li and J. Chen, *New J. Chem.*, 2025, DOI: 10.1039/D5NJ01943E.

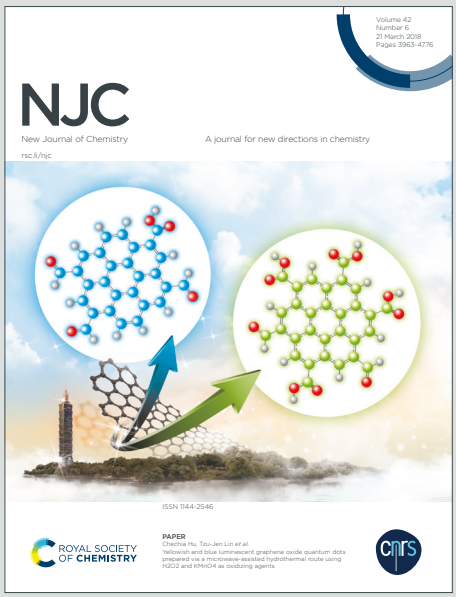

View Article Online
DOI: 10.1039/D5NJ01943E

ARTICLE

Solid-Phase Grinding Synthesis of Lead-Free $Cs_2Ag_{1-x}Na_xIn_{1-y}Bi_yCl_6$ Nanocrystals for Efficient Light Emission

Received 00th January 20xx,
Accepted 00th January 20xx

DOI: 10.1039/x0xx00000x

Enyu Zhan,[a] Fengchao Wang,[a] Jun Wang,*[ab] Yu Sun,[a] Jing Yang,[a] Canyun Zhang,[a] Jinfang Kong,[a] Lan Li[a], Jin Chen*[a]

In recent years, the lead-free halide perovskite has been extensively studied due to the the lead toxicity and poor stability of lead halide perovskite. $Cs_2AgInCl_6$ has shown great potential to replace lead halide perovskites in optoelectronic applications. However, this perovskite synthesis method needs to involve high temperature, the synthesis conditions are relatively harsh. In this work, a simple solid-phase grinding method was employed to prepare Na^+ and Bi^{3+} doped perovskite $Cs_2Ag_{1-x}Na_xIn_{1-y}Bi_yCl_6$ with systematically characterization of both the structure and optical performance. The experimental results showed that a photoluminescence quantum yield (PLQY) of 13.1% was achieved by breaking the parity-forbidden transition through 4% Bi^{3+} doping. Subsequently, the incorporation of 60% Na^+ suppressed non-radiative transitions and increased the PLQY to 56.9%. The $Cs_2Ag_{0.4}Na_{0.6}In_{0.96}Bi_{0.04}Cl_6$ samples were encapsulated on ultraviolet (UV) LED chips to obtain warm-yellow LED with good performances, which shows that promising applications in the LED field.

1. Introduction

In recent years, $APbX_3$ (A = MA^+, FA^+, Cs^+; X = Cl^-, Br^-, I^-) halide perovskite materials have become one of the most popular optoelectronic materials, they have the advantages of high photoluminescence quantum yield (PLQY), high carrier mobility, high defect tolerance, and tunable emission wavelength, which have led to the rapid development of lead halide perovskite materials.[1-5] Unfortunately, the inherent toxicity of Pb^{2+} can cause a certain amount of pollution to the environment and threaten human health, severely limiting its application in commercial equipment. Therefore, a new solution is needed to address environmental and health concerns.[6-10]

The less toxic Sn^{2+} and Ge^{2+} from the same group IV are usually considered to replace Pb^{2+}, however, unlike the stabilized Pb^{2+}, these materials are prone to oxidation to their respective 4^+ valence states in air, which leads to reduced stability and photovoltaic properties.[11-14] Another alternative to Pb^{2+} is to use the less easily oxidized trivalent cations Bi^{3+}, Sb^{3+}, but the Bi^{3+} and Sb^{3+} may lead to charge imbalance and structural deterioration of perovskite materials.[15-17] Thus, it is crucial to find stable, low-toxic and efficient perovskite.

Fully inorganic metal halide perovskite halide perovskite $A_2B(I)B(III)X_6$ is a promising class of lead-free semiconductor materials, which can replace lead-based perovskite in optoelectronic devices.[18] The elements at the B(I) position are monovalent cations, such as Na^+, K^+, Li^+, Ag^+, and Ru^+, the elements at the B(III) position are trivalent cations, such as Sb^{3+}, Bi^{3+}, In^{3+}, Ln^{3+}, Fe^{3+}. Among these materials, $Cs_2AgInCl_6$ perovskite demonstrates superior optical properties compared to other perovskite materials such as $Cs_2AgBiCl_6$, primarily attributed to its direct bandgap structure.[19-21] In recent years, the double perovskite $Cs_2AgInCl_6$ has been demonstrated to have a long carrier lifetime, relatively high stability, and unique Self-trapped exciton emission mechanism, which has brought it to the attention of researchers.[22, 23] Despite its many excellent properties, $Cs_2AgInCl_6$ has less absorption and emission in the visible and near-infrared regions, and its PLQY is relatively low, which is due to the parity-forbidden transition.[24] In order to improve the luminescent properties of $Cs_2AgInCl_6$, researchers have taken many approaches, among which, alloying or lattice doping is an effective method to improve the optical properties of $Cs_2AgInCl_6$. Tang's group investigated $Cs_2AgInCl_6$ and finally generated $Cs_2Ag_{1-x}Na_xInCl_6$ powder by hydrothermal reaction, the incorporation of alkali metal Na effectively modifies the symmetry of the electron wave function in self-trapped excitons, thereby breaking the parity-forbidden transition. Through Na^+ and Bi^{3+} doping, the PLQY of $Cs_2AgInCl_6$ powder was significantly enhanced to 86.2 ± 5%, and realized the warm-white luminescence of the sample.[25] Locardi and his colleagues synthesized Mn-doped $Cs_2AgInCl_6$ nanocrystals through a process comprising high-temperature heating, ice-bath cooling, and vacuum drying, achieving bright orange emission with a PLQY of 16%.[26] Liu synthesized well-dispersed $Cs_2AgInCl_6$: Bi nanocrystals via rapid injection of cesium oleate solution into HCl-containing precursors at 280°C. The resulting

a. College of Sciences, Shanghai Institute of Technology, 100 Haiquan Road, Shanghai 201418, China. E-mail: jinchenxl@sit.edu.cn
b. Shanghai MEICO Lighting Design Consulting Co., Ltd., Lane 399, Xinlong Road, Shanghai 201101, China. E-mail: meico_lighting@126.com
† Supplementary Information available: [details of any supplementary information available should be included here]. See DOI: 10.1039/x0xx00000x

View Article Online
DOI: 10.1039/D5NJ01943E

nanocrystals exhibited a broadband orange emission peak at 580 nm, with a PLQY of 11.4%.[27] It can be seen that although existing preparation strategies can synthesize lead-free perovskite with excellent luminescent properties, these synthesis methods need to involve high temperatures as well as the addition of concentrated HCL, which makes the synthesis conditions harsh and risky, therefore, there is a need to find a simple, low-cost synthesis method.

In this work, Na^+ and Bi^{3+} co-doped perovskite nanocrystals were synthesized via a facile solid-phase grinding method. This approach offers several advantages, requires no high-temperature heating and HCl, and it is easy to prepare on a large scale. Through 4% Bi^{3+} doping, the parity-forbidden transition was broken in $Cs_2AgIn_{0.96}Bi_{0.04}Cl_6$, resulting in a PLQY of 13.1%. Subsequent incorporation of 60% Na^+ further enhanced the PLQY to 56.9%, and the synthesized perovskite $Cs_2Ag_{0.4}Na_{0.6}In_{0.96}Bi_{0.04}Cl_6$ exhibited a broad emission spectrum and warm-yellow luminescence. Finally, the $Cs_2Ag_{0.4}Na_{0.6}In_{0.96}Bi_{0.04}Cl_6$ nanocrystals were successfully implemented as solid phosphors in light-emitting devices, demonstrating excellent performance and highlighting their potential for optoelectronic applications. This work provides valuable insights for further investigation of the optical properties of Na^+ and Bi^{3+} co-doped $Cs_2AgInCl_6$ materials.

2. Experimental details

2.1 Synthesis of $Cs_2Ag_{1-x}Na_xIn_{1-y}Bi_yCl_6$

CsCl (99.9%, Adamas-beta), AgCl (98%, Adamas-beta), NaCl (99.9%, Adamas-beta), $BiCl_3$ (analytical pure, Aladdin), $InCl_3$ (99.99%, Adamas-beta). All chemicals were used as received without further purification.

$Cs_2Ag_{1-x}Na_xIn_{1-y}Bi_yCl_6$ were synthesized by manual grinding. In a typical synthesis process, 2 mmol of CsCl, 1-x mmol of AgCl, x mmol of NaCl (x = 0, 0.2, 0.4, 0.6, 0.8 and 1.0), 1-y mmol of $InCl_3$ and y mmol of $BiCl_3$ (y = 0, 0.02, 0.04, 0.06, 0.08 and 0.1) were put into a mortar, then mixed and hand grinding 15-20 minutes. Finally, collecting the powder into the bottle for further characterization. The whole process was carried out at room temperature, and no solvent was added during the grinding process.

2.2 Characterizations

The PL, PLQY and Time-resolved PL experiments measurements were performed by using the OmniFluo900 fluorescence spectrophotometer (Beijing Zhuolihanguang Instrument Co., Ltd, China). Ultraviolet－visible (UV－Vis) absorption spectra were measured by a UV-2600 ultra-violet spectrophotometer (Shimadzu, Japan). The XRD analysis was performed on a D/max 2200PC X-ray diffractometer (Nikkei Electric Co., Ltd, Japan), with Cu K α radiation. An ESCALAB 250Xi X-ray photoelectron spectrometer (XPS) (Thermo Fisher Scientific, USA) was used to measure X-ray photoelectron spectra. A scanning electron microscope (SEM) (FEI, USA) was used to observe the morphology and element mapping image of perovskite crystals. Energy-dispersive spectroscopy (EDS) was used Oxford Xplore to evaluate the elemental ratios. High-resolution transmission electron microscopy (HRTEM) was performed using a JEOL JEM-2100 instrument.

3. Results and discussion

A series of $Cs_2Ag_{1-x}Na_xIn_{1-y}Bi_yCl_6$ were synthesized using the solid-phase milling method, as shown in Fig. 1a, the perovskite precursors were mixed in precise proportions and ground by hand in an agate mortar. Due to the direct contact between the grinding rod and the raw materials, mechanical energy is generated and transferred directly to the raw materials, resulting in a localized temperature increase in the particles. The temperature rise facilitates the mutual diffusion and penetration of the raw materials, thereby promoting chemical reactions and improving crystallinity. Fig. 1b displays the ground powder, which exhibits a warm-yellow emission under 365 nm illumination. Fig. 1c illustrates the structural model of Na-alloyed and Bi-doped $Cs_2AgInCl_6$ double perovskite, where the cubic unit cell framework is composed of $[BiCl_6]$, $[InCl_6]$, $[NaCl_6]$, and $[AgCl_6]$ octahedra.[25]

Scanning electron microscopy (SEM) was employed to examine the morphological changes in $Cs_2AgIn_{0.96}Bi_{0.04}Cl_6$ and $Cs_2Ag_{0.4}Na_{0.6}In_{0.96}Bi_{0.04}Cl_6$. Fig. 2a reveals that $Cs_2AgIn_{0.96}Bi_{0.04}Cl_6$ exhibits irregular shapes and some agglomeration. In contrast, Fig. 2b demonstrates that $Cs_2Ag_{0.4}Na_{0.6}In_{0.96}Bi_{0.04}Cl_6$ is relatively well dispersed with no significant agglomeration. We speculate that the addition of Na^+ facilitates the crystallization process. Additionally, energy-dispersive X-ray spectroscopy (EDS) mapping was performed to investigate the elemental distribution in $Cs_2Ag_{0.4}Na_{0.6}In_{0.96}Bi_{0.04}Cl_6$, as illustrated in Fig. 2c. The uniform distribution and overlap of all elements within the grains confirm the successful incorporation of Na^+ and Bi^{3+} into the $Cs_2AgInCl_6$ perovskite nanocrystals.

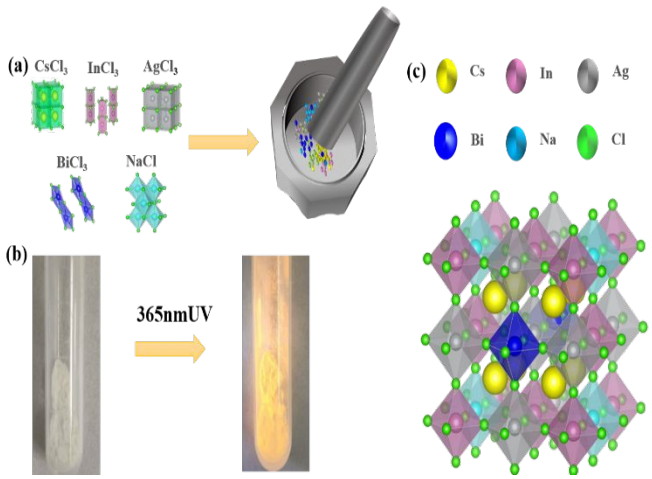

Fig. 1 (a) Synthesis process diagram of the $Cs_2Ag_{1-x}Na_xIn_{1-y}Bi_yCl_6$. (b) Photo of the $Cs_2Ag_{0.4}Na_{0.6}In_{0.96}Bi_{0.04}Cl_6$ sample and the sample under 365 nm UV light (c) The crystal structure of the $Cs_2Ag_{0.4}Na_{0.6}In_{0.96}Bi_{0.04}Cl_6$

View Article Online
DOI: 10.1039/D5NJ01943E

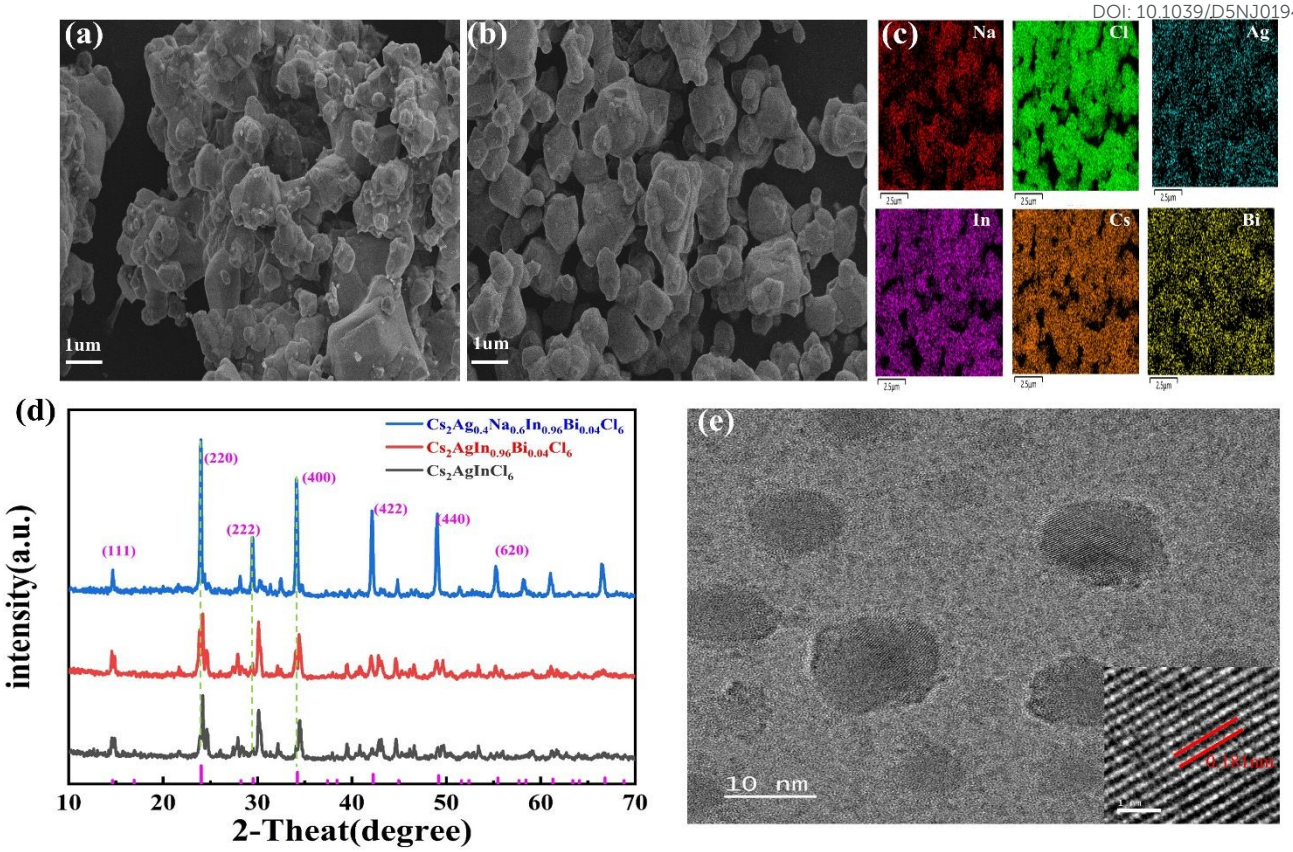

Fig. 2 SEM images of (a) $Cs_2AgIn_{0.96}Bi_{0.04}Cl_6$, (b) $Cs_2Ag_{0.4}Na_{0.6}In_{0.96}Bi_{0.04}Cl_6$. (c) EDS mapping of $Cs_2Ag_{0.4}Na_{0.6}In_{0.96}Bi_{0.04}Cl_6$. (d) XRD patterns of $Cs_2AgInCl_6$, $Cs_2AgIn_{0.96}Bi_{0.04}Cl_6$, and $Cs_2Ag_{0.4}Na_{0.6}In_{0.96}Bi_{0.04}Cl_6$ samples. (e) HRTEM of $Cs_2Ag_{0.4}Na_{0.6}In_{0.96}Bi_{0.04}Cl_6$ sample.

To investigate the effect of doping on the physical and structural properties of the samples, the perovskite nanocrystals were analyzed using X-ray diffraction (XRD) measurements. Fig. 2d presents the XRD patterns of $Cs_2AgInCl_6$, $Cs_2AgIn_{0.96}Bi_{0.04}Cl_6$ and $Cs_2Ag_{0.4}Na_{0.6}In_{0.96}Bi_{0.04}Cl_6$. The XRD patterns reveal that all perovskite nanocrystals exhibit a cubic FM-3m structure,[26] and mostly match that of the standard PDF of $Cs_2AgInCl_6$. As observed in Fig.2d, the diffraction peaks of (220), (222), (400) planes all move slightly to the low diffraction angle (2θ) with the doping of Bi^{3+} and Na^+ ions. This indicates the occurrence of lattice expansion which is caused by that Ag^+ (145pm) and In^{3+} (94pm) are replaced by Na^+ (166pm) and Bi^{3+} (117pm) with larger ionic radius, respectively. Compared to the standard XRD data, apart from the characteristic peaks that match the main peaks, there are impurity peaks in the synthesized samples, which may be due to trace amounts of unreacted precursors during the grinding process. Subsequently, we analyze the primary components of the impurity peaks in the XRD patterns, as shown in Fig. S1a, b. It can be seen that, aside from the diffraction peaks of $Cs_2AgInCl_6$, the other impurity peaks mainly correspond to AgCl and $InCl_3$, this is similar to previous studies.[9] It is noteworthy that after the introduction of Na^+, the intensity of the (220) peak gradually increases, and the impurity peaks decrease. This suggests that the incorporation of Na^+ effectively suppressed the formation of impurity phases and enhanced the crystallinity of the products, which is consistent with the SEM results shown above. In the HRTEM images (Fig. 2e) of $Cs_2Ag_{0.4}Na_{0.6}In_{0.96}Bi_{0.04}Cl_6$ sample, the $Cs_2Ag_{0.4}Na_{0.6}In_{0.96}Bi_{0.04}Cl_6$ nanocrystals are well-dispersed and homogeneous in morphology, which indicates that the perovskite nanocrystals have good structural integrity. Besides, $Cs_2Ag_{0.4}Na_{0.6}In_{0.96}Bi_{0.04}Cl_6$ perovskite nanocrystals has clearly visible lattice stripes, with a lattice spacing of 0.181 nm, this correspond to the (440) crystal surface of $Cs_2AgInCl_6$, which is a good confirmation of the doping of Na^+ and Bi^{3+}.

To further analyze the chemical composition and electronic structure of the samples, X-ray photoelectron spectroscopy (XPS) was performed on both $Cs_2AgIn_{0.96}Bi_{0.04}Cl_6$ and $Cs_2Ag_{0.4}Na_{0.6}In_{0.96}Bi_{0.04}Cl_6$. The XPS survey spectra (Fig. 3a-f) reveal characteristic peaks corresponding to Cs, Ag, In, Bi, and Cl in both materials. The distinct Na 1s peaks are observed in $Cs_2Ag_{0.4}Na_{0.6}In_{0.96}Bi_{0.04}Cl_6$. Fig. 3a confirms the successful incorporation of Na^+ ions. Notably, the Bi 4f (Bi $4f_{7/2}$ and Bi $4f_{5/2}$) and Cs 3d (Cs $3d_{5/2}$ and Cs $3d_{3/2}$) peaks exhibit a slight shift toward higher binding energies after Na^+ doping (Fig. 3b-c), which can be attributed to lattice expansion induced by Na^+ incorporation. Furthermore, the Cl 2p spectrum (Fig. 3d) demonstrates a significant shift of both Cl $2p_{1/2}$ and Cl $2p_{3/2}$ peaks to higher binding energies, likely resulting from the formation of $[NaCl_6]$ octahedra. In contrast, the binding energies of In 3d and Ag 3d orbitals remained unchanged (Fig.3e-f).

View Article Online
DOI: 10.1039/D5NJ01943E

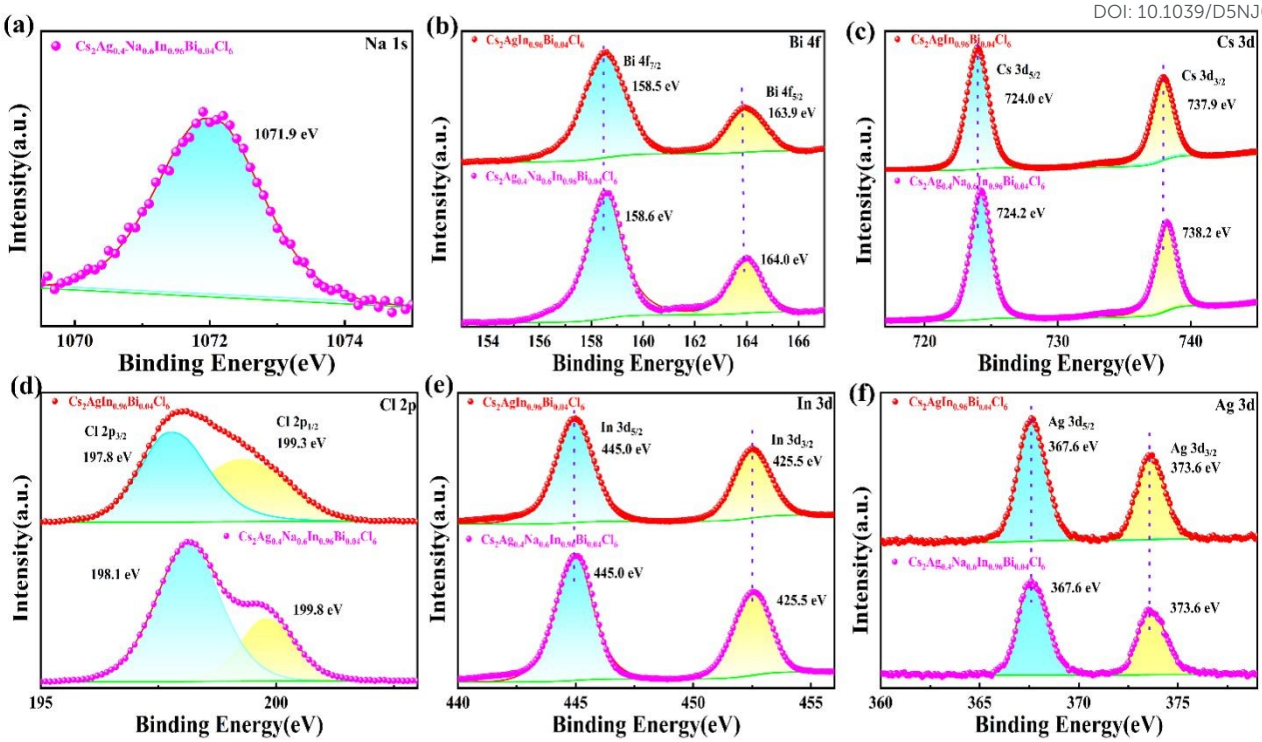

Fig. 3 Results of the XPS analyses conducted on $Cs_2AgIn_{0.96}Bi_{0.04}Cl_6$ and $Cs_2Ag_{0.4}Na_{0.6}In_{0.96}Bi_{0.04}Cl_6$. (a) Na 1s. (b) Bi 4f. (c) Cs 3d. (d) Cl 2p. (e) In 3d. (f) Ag 3d.

To investigate the effect of Bi^{3+} doping on the optical properties of $Cs_2AgInCl_6$ perovskite, UV-Vis absorption spectroscopy was conducted on $Cs_2AgIn_{1-y}Bi_yCl_6$. As shown in Fig. 4a, compared to the undoped $Cs_2AgInCl_6$, the Bi^{3+}-doped perovskite nanocrystals exhibit a sharp exciton absorption peak at 368 nm. The intensity of this peak gradually increases with higher Bi^{3+} concentrations, primarily due to the direct Bi s-p transition.[3] In contrast, $Cs_2AgInCl_6$ shows weak absorption at 368 nm, with more pronounced absorption occurring only below 350 nm. Based on the Tauc plot analysis, the optical bandgap of $Cs_2AgInCl_6$ is calculated to be 3.51 eV, consistent with previous studies and indicative of a direct bandgap.[28] In Fig. 4b, as the Bi^{3+} content increases, the bandgap of $Cs_2AgIn_{1-y}Bi_yCl_6$ gradually decreased from 3.13 eV to 2.88 eV. This reduction is attributed to the hybridization between the 6s orbitals of Bi and the 4d orbitals of Ag, which raises the valence band maximum (VBM) and consequently lowers the optical bandgap.[25]

Fig. 4c illustrates the emission spectra of $Cs_2AgIn_{1-y}Bi_yCl_6$ under 365 nm excitation, covering a spectral range of 400–800 nm, which is characteristic of broadband luminescent materials.[15] As the Bi^{3+} doping concentration increased from 0 to 0.04, the emission intensity of the samples gradually enhanced, reaching its maximum at a Bi^{3+} concentration of 4%, with a peak emission wavelength of 580 nm. Furthermore, the photoluminescence quantum yield (PLQY) achieved a maximum value of 13.1%, this is attributed to the incorporation of Bi^{3+} effectively breaks the parity-forbidden transition and generates additional excited-state electrons, thereby improving the absorption and excitation capabilities of the perovskite nanocrystals.[29, 30] However, when the Bi^{3+} doping concentration is further increased (y=0.06 to y=0.1), the emission intensity tends to weaken and the PLQY decreased (Fig. 4d), which is attributed to the concentration quenching effect. In addition, under the excitation of 365 nm, the center wavelength of the samples with different Bi^{3+} doping concentrations exhibited a red shift to varying degrees.

After successfully synthesizing the $Cs_2AgIn_{0.96}Bi_{0.04}Cl_6$ sample with optimal photoluminescence (PL) and photoluminescence quantum yield (PLQY) properties, we partially substituted Ag with Na to prepare $Cs_2Ag_{1-x}Na_xIn_{0.96}Bi_{0.04}Cl_6$ by systematically varying the x-value from 0 to 1 (x = 0, 0.2, 0.4, 0.6, 0.8, 1). As shown in Fig. 5a, with the increase of Na^+ concentration, the absorption peak of $Cs_2Ag_{1-x}Na_xIn_{0.96}Bi_{0.04}Cl_6$ gradually decrease and broaden. From the Tauc plot (Fig. 5b), the optical bandgap is observed to increase from 2.99 eV to 3.41 eV. In general, the broadband luminescence arises from self-trapped excitons (STEs), which are formed due to strong electron-phonon coupling in the material, and this coupling allows excited-state carriers to interact with the lattice, inducing lattice distortions and generating highly localized STEs, followed by radiative recombination.[25, 31, 32] In the excited state, STEs are generated through Jahn-Teller distortion of the $[AgCl_6]$ octahedra in $Cs_2AgIn_{0.96}Bi_{0.04}Cl_6$.[27, 33] In Fig. 5c, PL spectroscopy reveals that the intensity is significantly enhanced after Na^+ doping, exhibiting broadband emission characteristics. At x = 0.6, the PL intensity reach its maximum, with a PLQY as high as 56.9% (Fig. 5d). The PLQY of Na^+ and Bi^{3+} co-doped $Cs_2Ag_{1-x}Na_xIn_{0.96}Bi_{0.04}Cl_6$ significantly improves compared to Bi^{3+} doping alone.

View Article Online
DOI: 10.1039/D5NJ01943E

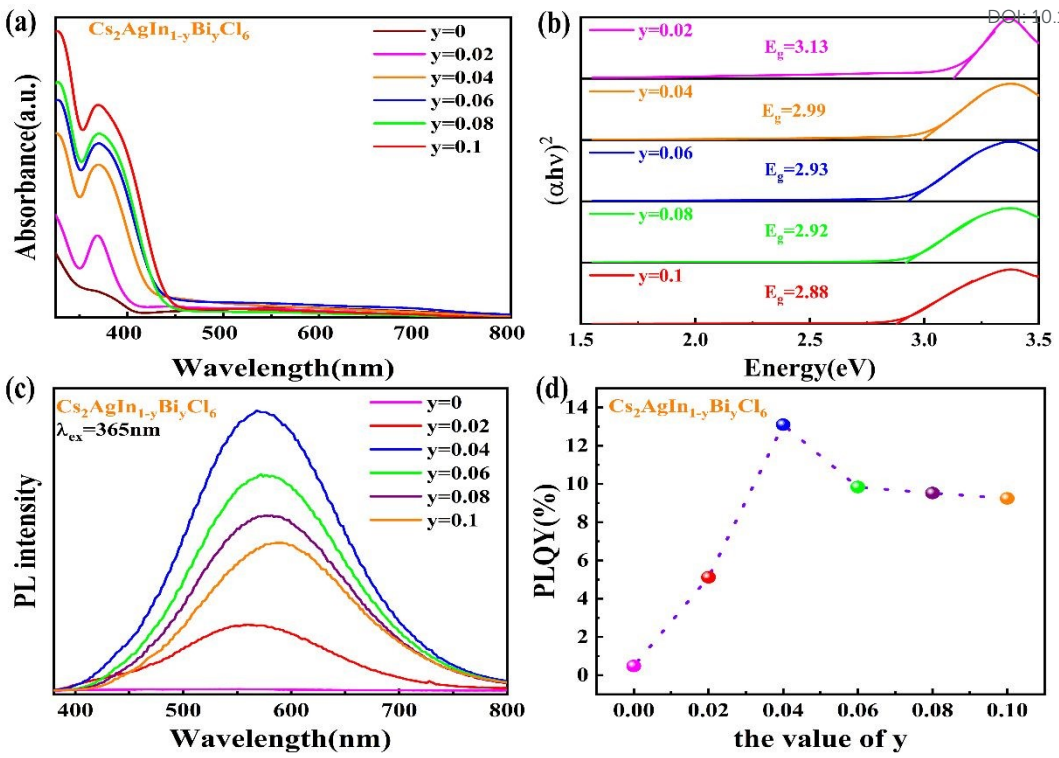

Fig. 4 Optical property of $Cs_2AgIn_{1-y}Bi_yCl_6$. (a) Optical absorption spectra of $Cs_2AgIn_{1-y}Bi_yCl_6$. (b) Tauc plots of $Cs_2AgIn_{1-y}Bi_yCl_6$. (c) PL spectra of $Cs_2AgIn_{1-y}Bi_yCl_6$ under the 365 nm ultraviolet irradiation. (d) PLQY of $Cs_2AgIn_{1-y}Bi_yCl_6$.

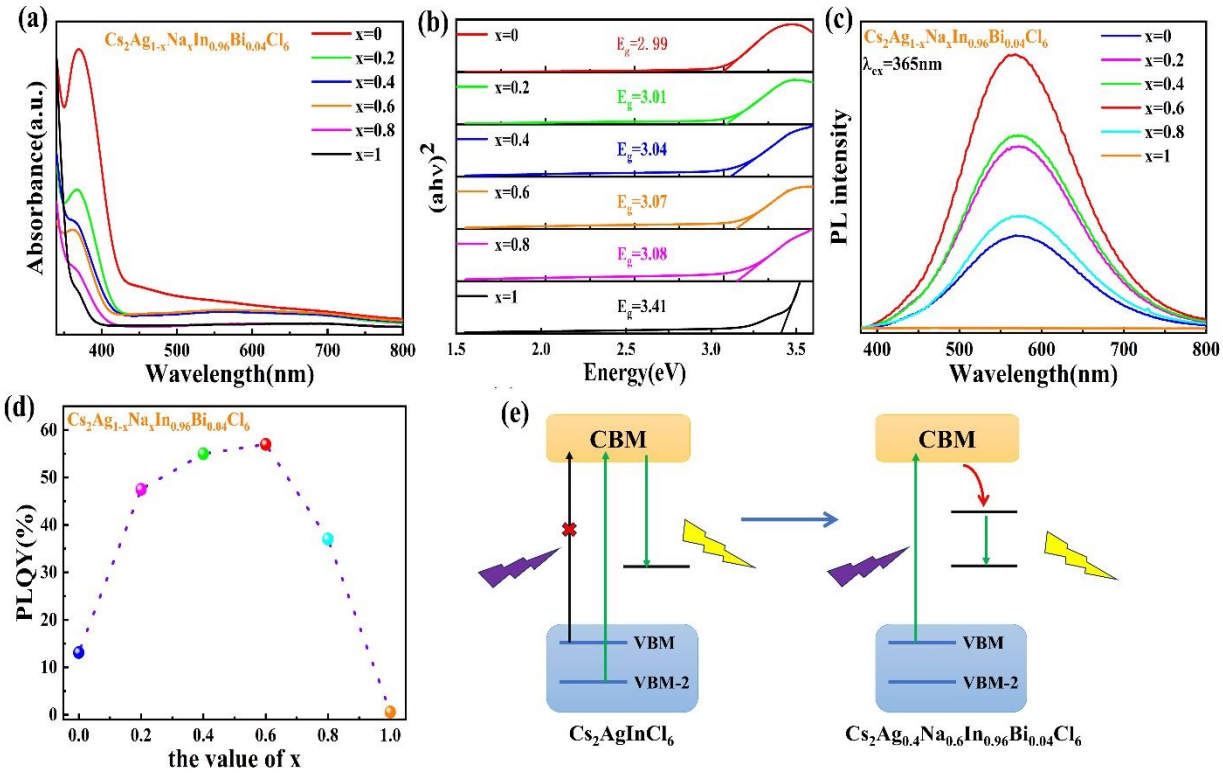

Fig. 5 Optical property of $Cs_2Ag_{1-x}Na_xIn_{0.96}Bi_{0.04}Cl_6$. (a) Optical absorption spectra of $Cs_2Ag_{1-x}Na_xIn_{0.96}Bi_{0.04}Cl_6$, (b) Tauc plots of $Cs_2Ag_{1-x}Na_xIn_{0.96}Bi_{0.04}Cl_6$. (c) PL spectra of $Cs_2Ag_{1-x}Na_xIn_{0.96}Bi_{0.04}Cl_6$ under the 365 nm ultraviolet irradiation. (d) PLQY of $Cs_2Ag_{1-x}Na_xIn_{0.96}Bi_{0.04}Cl_6$. (e) Emission mechanism of $Cs_2AgInCl_6$ and $Cs_2Ag_{0.4}Na_{0.6}In_{0.96}Bi_{0.04}Cl_6$

View Article Online
DOI: 10.1039/D5NJ01943E

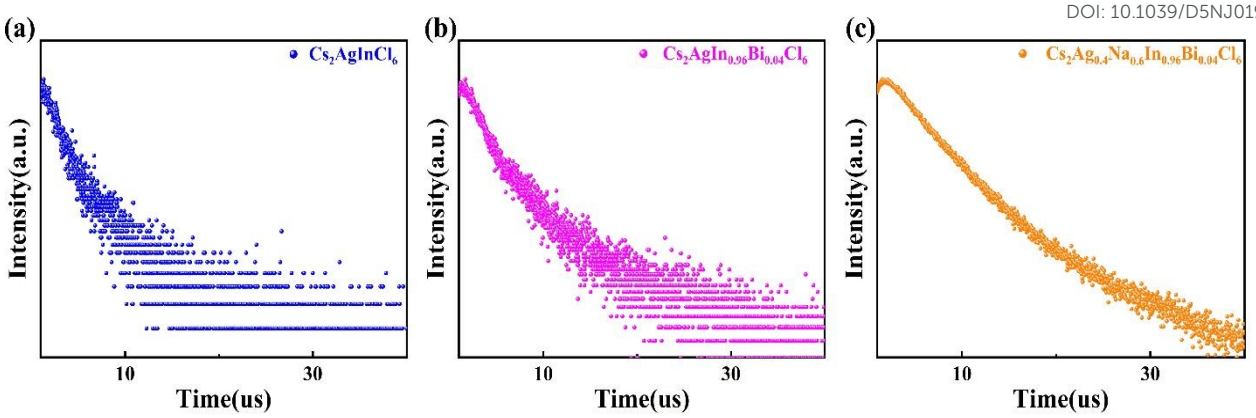

Fig.6 Time-resolved PL decay curves of (a) $Cs_2AgInCl_6$, (b) $Cs_2AgIn_{0.96}Bi_{0.04}Cl_6$, (c) $Cs_2Ag_{0.4}Na_{0.6}In_{0.96}Bi_{0.04}Cl_6$

Table 1 The fluorescence lifetime of $Cs_2AgInCl_6$, $Cs_2AgIn_{0.96}Bi_{0.04}Cl_6$, and $Cs_2Ag_{0.4}Na_{0.6}In_{0.96}Bi_{0.04}Cl_6$

Samples	A1	τ_1 (μs)	A2	τ_1 (μs)	τ_{ave}
$Cs_2AgInCl_6$	99%	1.85	1%	5.36	1.94
$Cs_2AgIn_{0.96}Bi_{0.04}Cl_6$	98%	2.49	2%	7.79	2.68
$Cs_2Ag_{0.4}Na_{0.6}In_{0.96}Bi_{0.04}Cl_6$	81%	3.86	19%	6.96	4.79

Compared to other perovskite systems such as $(BA)_2(MA)_{x-1}Pb_xBr_{3x+1}$,[34] $CsCu_2I_3$[35] and quasi-2D perovskite[36], the $Cs_2Ag_{0.4}Na_{0.6}In_{0.96}Bi_{0.04}Cl_6$ sample presents a good luminescent performance. However, compared to hydrothermally synthesized samples[25], $Cs_2Ag_{0.4}Na_{0.6}In_{0.96}Bi_{0.04}Cl_6$ exhibits a lower PLQY (56.9%), which may be attributed to relatively lower purity and the insufficient reaction in the prepared samples that compromise luminescence performance. The emission mechanism diagram of $Cs_2AgInCl_6$ perovskite nanocrystals before and after doping is shown in Fig. 5e. In pristine $Cs_2AgInCl_6$, the optical transition from the VBM to the CBM is parity-forbidden due to their identical parity symmetry. In contrast, the transition from VBM-2 to CBM is parity-allowed because of their opposite parity, which explains the intrinsically low PLQY of undoped $Cs_2AgInCl_6$ nanocrystals.[37, 38] The incorporation of Bi^{3+} effectively breaks the parity-forbidden transition between VBM and CBM in $Cs_2AgInCl_6$. This modification enhances the parity-allowed VBM to CBM transition, facilitating the generation of more free excitons and their subsequent efficient conversion into self-trapped exciton (STE) states.[27] Consequently, the STE emission intensity is significantly enhanced in Bi^{3+}-doped $Cs_2AgInCl_6$ nanocrystals. Furthermore, Na^+ doping induces partial isolation of the $[AgCl_6]$ octahedra, reducing the electronic dimensionality of the system. This disrupts the periodicity and local lattice symmetry of the crystal structure, further promoting the formation of STEs and thereby improving the overall luminescence efficiency.[30, 32]

Fig. 6a-c show the time-resolved PL (TRPL) decay spectra of $Cs_2AgInCl_6$, $Cs_2AgIn_{0.96}Bi_{0.04}Cl_6$, and $Cs_2Ag_{0.4}Na_{0.6}In_{0.96}Bi_{0.04}Cl_6$, and all the decay curves are well fitted by the following biexponential function, as shown in Eq1:

$$I(t) = A_1 \exp\left(-\frac{t_1}{\tau_1}\right) + A_2 \exp\left(-\frac{t_2}{\tau_2}\right) \quad (1)$$

where τ_1 refers to the short lifetime and τ_2 refers to the long lifetime. A1 and A2 are the corresponding amplitudes. According to the mentioned parameters, the average lifetime τ_{ave} can be calculated by the following equation (Eq2):

$$\tau_{ave} = \frac{A_1\tau_1^2 + A_2\tau_2^2}{A_1\tau_1 + A_2\tau_2} \quad (2)$$

Table 1 summarizes the fitted parameters obtained from the lifetime analysis. where τ_1 represents the non-radiative transition of free excitons and τ_2 corresponds to self-trapped excitons (STEs). The average lifetime (τ_{ave}) of $Cs_2AgIn_{0.96}Bi_{0.04}Cl_6$ (2.68 μs) shows a significant enhancement compared to that of undoped $Cs_2AgInCl_6$ (1.94 μs), As evident from Table 1, the contribution of τ_2 is negligible in the undoped samples of Na^+, τ_{ave} being predominantly governed by the non-radiative transition of free excitons. However, upon Na^+ incorporation, the proportion of τ_2 increases substantially, resulting in an extended τ_{ave} of 4.8 μs for $Cs_2Ag_{0.4}Na_{0.6}In_{0.96}Bi_{0.04}Cl_6$. This notable increase in τ_{ave} suggests enhanced STEs emission and effective suppression of non-radiative transitions in the Na^+-doped sample.[39]

In Fig. 7a, we investigated the variation of the PL spectra within the temperature range of 120K to 300K. As the temperature increases, the PL intensity of the sample continuously decreases, and the emission peak gradually blue shifts. This can be attributed to electron-phonon coupling and crystal lattice thermal expansion. To elucidate the intrinsic mechanism of temperature's effect on the PL intensity of $Cs_2Ag_{0.4}Na_{0.6}In_{0.96}Bi_{0.04}Cl_6$, we used the Arrhenius equation (3) to fit the curve of the integrated PL intensity as a function of

View Article Online
DOI: 10.1039/D5NJ01943E

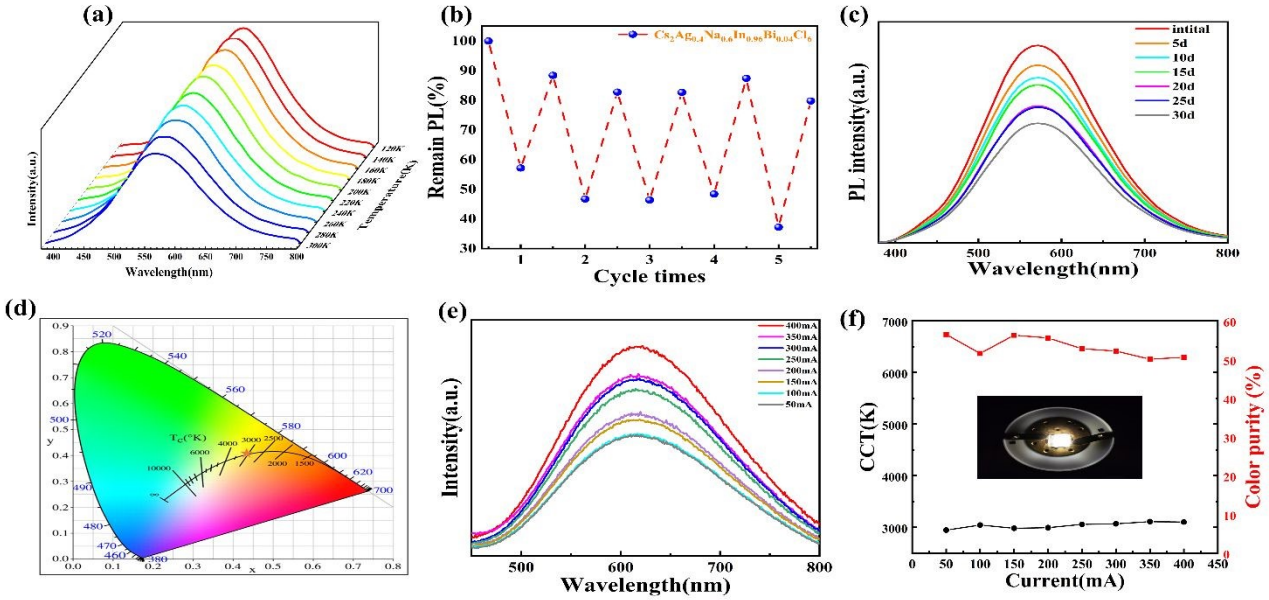

Fig. 7 (a)Photoluminescence spectra of $Cs_2Ag_{0.4}Na_{0.6}In_{0.96}Bi_{0.04}Cl_6$ measured at different temperatures from 120 to 300 K. (b)Heating/cooling PL tests of the $Cs_2Ag_{0.4}Na_{0.6}In_{0.96}Bi_{0.04}Cl_6$ sample at a temperature of 20–100 °C. (c) PL spectra of $Cs_2Ag_{0.4}Na_{0.6}In_{0.96}Bi_{0.04}Cl_6$ measured at fixed interval (5 days) in 30 days. (d) CIE chart of the $Cs_2Ag_{0.4}Na_{0.6}In_{0.96}Bi_{0.04}Cl_6$ sample. (e) Emission spectra of the LED at a driving current from 50 to 400 mA. (f) The variation of CCT and color purity with driving currents. The inset is the photo of the LED device.

temperature and calculated the exciton binding energy of $Cs_2Ag_{0.4}Na_{0.6}In_{0.96}Bi_{0.04}Cl_6$.

$$I(t) = A_1 \exp\left(-\frac{t_1}{\tau_1}\right) + A_2 \exp\left(-\frac{t_2}{\tau_2}\right) \quad (3)$$

Here, I_0 represents the PL intensity at 0 K, A is the fitting constant, E_b is the exciton binding energy, and K_b is the Boltzmann constant. The fitting results show (Fig. S2) that the exciton binding energy (E_b) of $Cs_2Ag_{0.4}Na_{0.6}In_{0.96}Bi_{0.04}Cl_6$ nanocrystals is 87.06 meV (Fig. S3). Generally speaking, a larger exciton binding energy can enhance the stability of excitons at room temperature or even higher, which has a positive impact on their luminescent performance.

In order to investigate the effect of heat on the stability of $Cs_2Ag_{0.4}Na_{0.6}In_{0.96}Bi_{0.04}Cl_6$ samples, thermal cycling tests were conducted in an air environment (20°C-100°C), and the residual PL intensity after each cycle was recorded. As shown in Fig. 7b, as the temperature increases, the fluorescence intensity decreases due to quenching, but the intensity recovers after the sample cools down. After five cycles, the sample still retains 80% of its relative emission intensity, demonstrating good stability.

A stability research of the photoluminescence (PL) stability of $Cs_2Ag_{0.4}Na_{0.6}In_{0.96}Bi_{0.04}Cl_6$ was characterized through 30-day tests under 365 nm UV illumination. The Fig. 7c depicts a 40.2% decrease in PL intensity. This decline may be due to the ionic nature of $Cs_2Ag_{0.4}Na_{0.6}In_{0.96}Bi_{0.04}Cl_6$, which leads to decomposition under continuous humidity, oxygen, heating, or irradiation conditions,[40, 41] adversely affecting carrier transport and recombination processes, thereby reducing the performance of sample. In order to investigate the potential application of this material in the field of LED, we selected the sample with the best luminescence performance, $Cs_2Ag_{0.4}Na_{0.6}In_{0.96}Bi_{0.04}Cl_6$, and prepared LED by combining the $Cs_2Ag_{0.4}Na_{0.6}In_{0.96}Bi_{0.04}Cl_6$ powder with commercial UV-emitting LED chips (365 nm). Fig. 7d shows that the $Cs_2Ag_{0.4}Na_{0.6}In_{0.96}Bi_{0.04}Cl_6$-based LED device exhibits stable luminescence characteristics in the warm-yellow light region at 100 mA, with the CIE color coordinates maintained (0.43,0.40), the correlated color temperature (CCT) of 3044 K and the color rendering index (CRI) of 89.3. Table. S1 shows that the color characteristics of $Cs_2Ag_{0.4}Na_{0.6}In_{0.96}Bi_{0.04}Cl_6$, among them, the luminous efficacy is lower than previously reported,[42, 43] and this can be improved through packaging process. In order to further evaluate its optoelectronic performance, we investigated the device performance under different driving currents (50-400 mA). As shown in the Fig. 7e, the luminescence intensity shows a stable growth trend with the increase of the driving current, and no premature saturation phenomenon of UV excitation occurs. Moreover, Fig. 7f shows that the CCT and color purity are almost unchanged under the effect of different driving currents, the inset is the photo of the LED device. This experimental result show that lead-free halide perovskite materials developed in this study exhibit excellent optoelectronic properties and have the potential to replace conventional lead-based halide perovskite for optoelectronic device applications.

Conclusions

In summary, this study successfully synthesized lead-free $Cs_2AgInCl_6$ double perovskite nanocrystals via a simple solid-phase grinding method, and the $Cs_2AgInCl_6$ perovskite were modified by Bi^{3+} doping and Na^+ doping, which broke the parity-forbidden transition of $Cs_2AgInCl_6$, achieving highly efficient and stable full-spectrum emission of visible light. Experimental

results demonstrated optimal luminescence efficiency (56.9%) with 4% Bi^{3+} and 60% Na^{+} doping concentrations. The optimized $Cs_2Ag_{0.4}Na_{0.6}In_{0.96}Bi_{0.04}Cl_6$ was encapsulated onto commercial UV LED chips to fabricate functional devices, exhibiting CIE coordinates of (0.43, 0.40), a correlated color temperature (CCT) of 3044 K, and a color rendering index (CRI) of 89.3. The fabricated LED maintained excellent stability under varying operating currents. These findings highlight the potential of lead-free double perovskites as environmentally friendly alternatives to lead-based perovskites in optoelectronic applications, offering superior luminescent efficiency and remarkable stability.

Conflicts of interest

There are no conflicts to declare.

Data availability

The data that support the findings of this study are available from the corresponding author upon reasonable request.

Acknowledgements

The project was sponsored by Shanghai Sailing Program, China (No. 20YF1447600), AI-enabled discipline promotion plan of Shanghai, China (No. AIZX-10), Collaborative innovation project of Shanghai Institute of Technology (No. XTCX2023-22), and Science and Technology Talent Development Fund for Young and Middle-aged Teachers of Shanghai Institute of Technology (No. ZQ2022-6).

Notes and references

1 L. Protesescu, S. Yakunin, M. I. Bodnarchuk, F. Krieg, R. Caputo, C. H. Hendon, R. X. Yang, A. Walsh and M. V. Kovalenko, *Nano Lett*, 2015, 15, 3692-3696.
2 D. Y. Han, J. Wang, L. Agosta, Z. Zang, B. Zhao, L. M. Kong, H. Z. Lu, I. Mosquera-Lois, V. Carnevali, J. C. Dong, J. H. Zhou, H. Y. Ji, L. Pfeifer, S. M. Zakeeruddin, Y. G. Yang, B. Wu, U. Rothlisberger, X. Y. Yang, M. Grätzel and N. Wang, *Nature*, 2023, 622, 493.
3 Y. Bekenstein, J. C. Dahl, J. Huang, W. T. Osowiecki, J. K. Swabeck, E. M. Chan, P. Yang and A. P. Alivisatos, *Nano Lett*, 2018, 18, 3502-3508.
4 I. Levchuk, A. Osvet, X. Tang, M. Brandl, J. D. Perea, F. Hoegl, G. J. Matt, R. Hock, M. Batentschuk and C. J. Brabec, *Nano Lett*, 2017, 17, 2765-2770.
5 B. A. Koscher, J. K. Swabeck, N. D. Bronstein and A. P. Alivisatos, *J. Am. Chem. Soc.*, 2017, 139, 6566-6569.
6 J. Xu, G. Chen, T. Yang, H. Wu, L. Li, C. Ma, C. Zhu, Y. Wu, B. Liu, A. Hu, X. Qiu, L. Zhong, J. Shen, A. Huang, Y. Guo and H. Gao, *Journal of Luminescence*, 2023, 255,119606.
7 Y. C. Ling, Z. Yuan, Y. Tian, X. Wang, J. C. Wang, Y. Xin, K. Hanson, B. W. Ma and H. W. Gao, *Adv. Mater.*, 2016, 28, 305-311.
8 W. J. Mir, A. Warankar, A. Acharya, S. Das, P. Mandal and A. Nag, *Chem. Sci.*, 2017, 8, 4602-4611.
9 H. Wang, J. Chen, Y. Sun, F. Wang, J. Yang, C. Zhang, J. Kong and L. Li, *Sci. Rep.*, 2024, 14, 14740.
10 M. H. Wang, W. Wang, B. Ma, W. Shen, L. H. Liu, K. Cao, S. F. Chen and W. Huang, *Nano-Micro Lett.*, 2021, 13, 36.
11 M. Q. Lyu, J. H. Yun, P. Chen, M. M. Hao and L. Z. Wang, *Adv. Energy Mater.*, 2017, 7, 26.
12 K. Dave, M. H. Fang, Z. Bao, H. T. Fu and R. S. Liu, *Chem.-Asian J.*, 2020, 15, 242-252.
13 S. Yang, S. Huang, Q. Wang, R. Wu, Q. Han and W. Wu, *Optical Materials*, 2019, 98,109444.
14 F. Locardi, E. Sartori, J. Buha, J. Zito, M. Prato, V. Pinchetti, M. L. Zaffalon, M. Ferretti, S. Brovelli, I. Infante, L. De Trizio and L. Manna, *ACS Energy Letters*, 2019, 4, 1976-1982.
15 Y. Liu, A. Nag, L. Manna and Z. Xia, *Angew. Chem. Int. Ed. Engl.*, 2021, 60, 11592-11603.
16 L. Chu, W. Ahmad, W. Liu, J. Yang, R. Zhang, Y. Sun, J. P. Yang and X. A. Li, *Nano-Micro Lett.*, 2019, 11, 18.
17 N. K. Tailor, A. Listorti, S. Colella and S. Satapathi, *Adv. Mater. Technol.*, 2023, 8, 15.
18 Z. Z. Ma, L. T. Wang, X. Z. Ji, X. Chen and Z. F. Shi, *J. Phys. Chem. Lett.*, 2020, 11, 5517-5530.
19 J. Zhou, Z. Xia, M. S. Molokeev, X. Zhang, D. Peng and Q. Liu, *J. Mater. Chem. A*, 2017, 5, 15031-15037.
20 S. Yang, F. Wang, L. Li, C. Zhang, J. Kong, J. Chen and Y. Dou, *Optical Materials*, 2023, 139,113748.
21 F. He, Y. Wang, T. Debnath, M. Döblinger, Q. A. Akkerman, J. Feldmann and A. Dey, *Adv. Opt. Mater.*, 2024, 12,2302898.
22 J. Luo, S. Li, H. Wu, Y. Zhou, Y. Li, J. Liu, J. Li, K. Li, F. Yi, G. Niu and J. Tang, *ACS Photonics*, 2017, 5, 398-405.
23 X. Huang, Y. Matsushita, H. T. Sun and N. Shirahata, *Nanoscale Adv.*, 2022, 4, 3091-3100.
24 W. Meng, X. Wang, Z. Xiao, J. Wang, D. B. Mitzi and Y. Yan, *J. Phys. Chem. Lett.*, 2017, 8, 2999-3007.
25 J. Luo, X. Wang, S. Li, J. Liu, Y. Guo, G. Niu, L. Yao, Y. Fu, L. Gao, Q. Dong, C. Zhao, M. Leng, F. Ma, W. Liang, L. Wang, S. Jin, J. Han, L. Zhang, J. Etheridge, J. Wang, Y. Yan, E. H. Sargent and J. Tang, *Nature*, 2018, 563, 541-545.
26 F. Locardi, M. Cirignano, D. Baranov, Z. Dang, M. Prato, F. Drago, M. Ferretti, V. Pinchetti, M. Fanciulli, S. Brovelli, L. De Trizio and L. Manna, *J. Am. Chem. Soc.*, 2018, 140, 12989-12995.
27 Y. Liu, Y. Jing, J. Zhao, Q. Liu and Z. Xia, *Chem. Mater.*, 2019, 31, 3333-3339.
28 T. T. Tran, J. R. Panella, J. R. Chamorro, J. R. Morey and T. M. McQueen, *Materials Horizons*, 2017, 4, 688-693.
29 Y. Zhang, Z. Zhang, W. Yu, Y. He, Z. Chen, L. Xiao, J. j. Shi, X. Guo, S. Wang and B. Qu, *Adv. Sci.*, 2021, 9,2102895.
30 S. Jin, H. Yuan, T. Pang, M. Zhang, Y. He, B. Zhuang, T. Wu, Y. Zheng and D. Chen, *Adv. Funct. Mater.*, 2023, 33.
31 M. B. Gray, J. D. Majher, T. A. Strom and P. M. Woodward, *Inorg. Chem.*, 2019, 58, 13403-13410.
32 S. Li, J. Luo, J. Liu and J. Tang, *J. Phys. Chem. Lett.*, 2019, 10, 1999-2007.
33 B. Yang, X. Mao, F. Hong, W. Meng, Y. Tang, X. Xia, S. Yang, W. Deng and K. Han, *J. Am. Chem. Soc.*, 2018, 140, 17001-17006.
34 J. Wang, X. Liu, L. Zhou, W. Shen, M. Li and R. He, *Nanoscale Adv.*, 2021, 3, 5393-5398.
35 B. Wang, Y. Tang, X. Yang, W. Cai, R. Li, W. Ma, S. Zhao, C. Chen and Z. Zang, *Nano Mater. Sci.*, 2023, 5, 78-85.
36 J. Wang, D. Li, J. Wang and J. Peng, *Mater. Futures*, 2022, 1,045301.

View Article Online
DOI: 10.1039/D5NJ01943E

37 A. H. Slavney, T. Hu, A. M. Lindenberg and H. I. Karunadasa, *J. Am. Chem. Soc.*, 2016, 138, 2138-2141.
38 X. K. Gong, X. S. Zhang, X. Liu, R. K. Ding, J. J. Zhang, H. Yin, Z. W. Zhang, L. Li and J. P. Xu, *J. Hazard. Mater.*, 2021, 403, 123821.
39 Q. Hu, G. Niu, Z. Zheng, S. Li, Y. Zhang, H. Song, T. Zhai and J. Tang, *Small*, 2019, 15, e1903496.
40 S. Khalfin and Y. Bekenstein, *Nanoscale*, 2019, 11, 8665-8679.
41 H. Tang, Y. Xu, X. Hu, Q. Hu, T. Chen, W. Jiang, L. Wang and W. Jiang, *Adv. Sci. (Weinh.)*, 2021, 8, 2004118.
42 Y. Yue, H. Zhu, C. Dzorkpata, Y. Chen and P. Zhu, IEEE *Trans. Electron Devices*, 2025, 72, 728-734.
43 Y. Chen, H. Zhu, D. Babaian, C. Dzorkpata, A. Grigoriev, Z. Wang, S. Wheat, S. Guha and P. Zhu, *Adv. Mater.*, 2025, 37, 2500083.

View Article Online
DOI: 10.1039/D5NJ01943E

The data that support the findings of this study are available from the corresponding author upon reasonable request.